



Article

# Acoustic Emission Damage Detection during Three-Point Bend Testing of Short Glass Fiber Reinforced Composite Panels: Integrity Assessment

Hadi Nazaripoor<sup>1</sup>, Hossein Ashrafizadeh<sup>1</sup> , Ryan Schultz<sup>1</sup>, Joel Runka<sup>1</sup> and Pierre Mertiny<sup>2,\*</sup>

<sup>1</sup> Shawcor Composite Production Systems, 3501 54th Ave SE, Calgary, AB T2C 0A9, Canada; hadi.nazaripoor@shawcor.com (H.N.); ashrafiz@ualberta.ca (H.A.); ryan.schultz@shawcor.com (R.S.); joel.runka@shawcor.com (J.R.)

<sup>2</sup> Department of Mechanical Engineering, University of Alberta, Edmonton, AB T6G 1H9, Canada

\* Correspondence: pmertiny@ualberta.ca

**Abstract:** In this study, an acoustic emission (AE) technique was used as a passive non-destructive tool to detect the damage progress in short glass fiber-reinforced composite panels. AE detection was conducted during three-point bend tests, thus illustrating the flexural damage accumulation for composite panels with different sizes and fiber volume content. To demonstrate the universality of the employed integrity assessment methodology, AE data was detected using different timing parameters and two different transducer types, i.e., medium-band and wide-band frequency sensors. The AE waveform classification presented in this study is based on peak frequency distributions. Frequency bands that are associated with certain failure mechanisms, including matrix micro-cracking, fiber debonding, delamination, and fiber breakage, were obtained from the technical literature. Through this investigation, the concept of cumulative signal strength (CSS) and cumulative rise time versus peak amplitude ratio (CRA) as AE output parameters are shown to facilitate integrity assessment for the employed complex composite material system. Significant jumps in CSS and CRA curves could be correlated to critical strain levels and distinct damage events in the composite panels subjected to flexural loading.

**Keywords:** integrity assessment; acoustic emission; damage detection; cumulative signal strength; short fiber polymer composites; flexural testing



**Citation:** Nazaripoor, H.; Ashrafizadeh, H.; Schultz, R.; Runka, J.; Mertiny, P. Acoustic Emission Damage Detection during Three-Point Bend Testing of Short Glass Fiber Reinforced Composite Panels: Integrity Assessment. *J. Compos. Sci.* **2022**, *6*, 48. <https://doi.org/10.3390/jcs6020048>

Academic Editor:  
Francesco Tornabene

Received: 29 November 2021

Accepted: 30 January 2022

Published: 3 February 2022

**Publisher's Note:** MDPI stays neutral with regard to jurisdictional claims in published maps and institutional affiliations.



**Copyright:** © 2022 by the authors. Licensee MDPI, Basel, Switzerland. This article is an open access article distributed under the terms and conditions of the Creative Commons Attribution (CC BY) license (<https://creativecommons.org/licenses/by/4.0/>).

## 1. Introduction

Advancements in the design and manufacturing of composite materials have rendered reinforced polymer composite (RPC) materials a competitive candidate for a variety of engineering, industrial and technological applications, in sectors, such as aerospace, military, civil engineering and construction, oil and gas exploration, and chemical processing. High specific mechanical stiffness and strength, high resistance against corrosion, low weight, and improved fatigue performance are a few attractive characteristics of RPCs. Additionally, the composition of a fiber-reinforced polymer composite (FRPC) can be tailored to optimize component weight and rigidity. The present study was conducted on the background of FRP pipes and vessels. In chemically reactive environments, corrosion damage in traditional steel and concrete pipes and tanks necessitates costly repairs and maintenance efforts, which buoys the demand for FRPC products that are highly resistant to corrosion, while not sacrificing pressure loading capacity. Reduced costs in production, installation and repair are other attractive properties of FRP pipes and vessels compared to their traditional competitors.

An FRPC consists of a polymer matrix with embedded reinforcing elements, such as glass, carbon, and aramid fibers, to mention a few. In the context of FRP pipes and tanks, thermoset polymers are commonly employed. The primary functions of the polymer matrix

phase are to bind the composite fiber architecture, provide rigidity to the components, facilitate a load share between reinforcement fibers, and prevent fluid leakage from the interior of tanks or vessels. The matrix also protects the load-bearing fibers from corrosive and mechanical degradation in abrasive and chemically harsh environments.

FRP materials may suffer structural failure when applied loads (i) exceed fiber strength leading to fiber fracture, (ii) cause fiber debonding from the polymer matrix due to shear or peeling at the interface between fiber and matrix, and (iii) exceed the strength of the matrix resulting in matrix cracking [1]. Polymer matrix cracking is characterized by the fracturing of the polymer matrix in between and along the fibers. Other damage modes include fiber buckling under compressive loadings. Due to the inhomogeneity of FRPC structures, complex damage behavior, including micro-cracking of the polymer matrix, is typically observed, which, in pressure-bearing composite structures, may lead to fluid leakage [2]. Over time and under continued loading, fractures accumulate and coalesce, affecting stiffness properties and providing for fluid pathways leading to leakage. This functional damage mode is often termed “weepage” and occurs at load levels well below a collapse failure or structural burst of a composite pipe or tank. Moreover, the damage behavior and, thus, performance of FRPC structures also depends on the temperature regime because polymer properties are strongly affected by comparatively moderate temperature changes.

The safety and reliability of pressurized systems have been of great public concern since the start of the industrial age [3]. Using structural health monitoring (SHM) methods can mitigate such concerns and avoid overly conservative and, thus, costly design approaches. Non-destructive testing and evaluation (NDT&E) is an integral part of SHM systems. Several NDT&E methods, such as acoustic emission (AE), ultrasonic testing, and infrared thermography, are used to monitor structural performance, including displacements, strains, and even stresses [4,5]. Output data by such a system is post-processed to infer the structure’s current operational state and remaining life.

AE detection is a valuable technique for monitoring damage in composites and identifying damage locations. An abrupt localized strain change within a body engenders transient mechanical waves called acoustic emissions [6]. Crack growth, even a minute propagation, and similar flaws are mechanisms by which abrupt strain changes occur in FRPC (i.e., in a fiber, the polymer matrix, or both). The resulting surface elastic-wave motion with sufficient amplitude can be detected using sensors (transducers) attached to the surface. The sensors convert a mechanical disturbance to an electric (voltage-time) waveform sent to a post-processing analyzer [7]. Thus, the surface signal from an AE source can be analyzed to extract information about its characteristics and location, including damage initiation and existing damage propagation events within a material.

Three aspects are distinctive for AE wave propagation-based SHM techniques compared to other SHM methods: (1) minimum instrumentation is needed for large area monitoring; (2) damage locations can be identified; and (3) global monitoring is possible since the energy required for sensing originates from the damage-source. Notably, the International Atomic Energy Agency considers AE an appropriate method and recommends it for inspection [8,9]. AE has widely been used for metallic structures and FRPC products in engineering and technological applications. However, due to a diverse range of possible inhomogeneous material compositions and the anisotropic nature of FRPC materials, AE techniques need to be adapted to capture more intricate wave signals and identify a more extensive variety of damage modes [10]. Hence, data processing in AE is not a trivial task as each application requires a specific interpretation of the recorded acoustic signals relying on the underlying physical phenomena. Over the past decade, with enhancements in computation and data analysis capacities, there have been remarkable works focusing on the AE signal characterization and damage identification using (i) a single parameter classification, such as amplitude, frequency, or wavelet level, (ii) multiple parameters classification using pattern recognition techniques, and (iii) classification based on the extensional and flexural mode content or modal analysis.

Amplitude-based classification has received significant attention in the past. However, from various studies on AE on unidirectional and cross-ply carbon/epoxy composites, the amplitude range and associated damage modes (including matrix micro-cracking and fiber fracture) were inconclusive. In addition, it was observed that the sensor distance significantly altered the measured amplitude, suggesting using the peak frequency of AE signals instead [11]. More recently, the frequency content of AE signals has been used to classify failure modes. Examining un-cured and cured carbon/epoxy laminates, as well as pure epoxy, in Reference [12], and tensile tests of several ply orientations using a glass/polypropylene system, in Reference [13], revealed fiber failure to be in the high-frequency range and fiber pull-out in the intermediate frequency range. Matrix cracking was also in the low-frequency range, while delamination has a frequency range between fiber pull-out and fiber fracture [12]. A summary of the identified damage modes in glass fiber (GF)- or carbon fiber (CF)- reinforced thermoset composite structures is presented in Table 1. These results are based on waveform analysis and frequency content of detected AE signals (also called ‘hits’). Although there is a difference in reported frequency ranges for each damage mode due to the difference in material types and dissimilarity of AE detection systems used in the technical literature, clear distinctions between damage mechanisms are apparent.

**Table 1.** Summary of identified damage modes in FRPCs based on frequency and waveform analysis, GF: glass fiber, CF: carbon fiber.

Literature	Fiber/Matrix Type	Frequency Range for Each Failure Mode (kHz)			
		Matrix Cracking	Fiber-Matrix Debonding	Delamination	Fiber Breakage
[14]	GF/polyester	100–150	150–250	<120	350–500
[15]	GF/epoxy	50–200	-	-	-
[13]	GF/polypropylene	-	90–110	-	420–540
[16]	GF/epoxy	100–190	-	200–320	380–430
[17]	GF/epoxy	<60	-	200–320	380–430
[18]	GF/epoxy	62.5–125	125–187.5	-	187.5–250
[12]	CF/epoxy	50–180	220–300	220–300	300–530
[19]	CF/epoxy	80–130	160–190	130–160	190–330
[20]	CF/epoxy	<50	50–150	200–300	400–500

Employing more advanced artificial intelligence-based pattern recognition techniques [18,20–29] that rely on the classification of several parameters (rise times, amplitudes, energy, peak frequency, etc.) into cluster forming patterns also received considerable attention. Correlations between direct optical observations and AE signal parameter classification in CF-reinforced composite laminates indicated that matrix cracking also resulted in high frequency signals [27]. The performance of different unsupervised or supervised clustering methods that have been used by researchers is highly dependent on the structure of the AE recorded data. AE features, such as amplitude, duration, rise time, energy, counts, and peak frequency, are affected by the sensor type (medium band or wideband), specimen geometry and composite lay-up, continuous or discontinuous fiber reinforcement, and AE timing parameters, i.e., threshold level, peak detection time (PDT), hit detection time (HDT), and hit lock time (HLT) [28,29]. All of these factors should be considered while comparing the results available in the literature. In the present study, the focus is on finding a reliable quantitative approach for integrity assessment of composite structures, rather than damage diagnosis.

In this experimental work, the AE response during three-point bend testing of short glass fiber-reinforced thermoset composite (SFRC) panels was investigated, aiming at the integrity assessment of such complex material systems during loading. In what follows, first, the materials and methods used to investigate the AE response during flexural loading of SFRC panels are described. The universality of the employed methodology is demonstrated

by capturing AE data using different timing parameters and two different transducer types, i.e., medium-band and wide-band frequency sensors. Second, the mechanical properties and the damage modes in the tested samples are discerned and discussed. Included herein are AE signal properties recorded during the testing campaign. The dynamics of the damage progress is explored using an AE-based characteristic feature as an integrity assessment approach (i.e., cumulative signal strength (CSS)). Lastly, AE data are presented considering different AE features, i.e., amplitude, duration, peak frequency, weighted peak frequency, rise time, and rise time versus peak amplitude ratio (RA). This study introduces a redefined RA parameter and the cumulative RA (CRA) as integrity assessment features that can be used similarly to the CSS to characterize the damage progression in SFRC panels.

## 2. Materials and Methods

### 2.1. Materials

Mechanical testing and AE monitoring was performed on two sets of short glass fiber-reinforced polyester composite panel coupons, one set with a fiber volume fraction of 12.5%, and the other with 15%. Composite panels for testing were fabricated by manual spray-up technique, resulting in random fiber orientations. The exact polymer composition and fiber type are proprietary. Coupon specimens for bend testing were water jet cut from the panels. After cutting, all edges were polished using wet sandpaper (180 and 320 grit). Specimen dimensions are summarized in Table 2. Long beam flexure properties and the fiber content were derived based on the ASTM D7264 [30] and ASTM D2584 [31] standards, respectively.

**Table 2.** Summary of short glass fiber-reinforced polyester composite panel coupons.

Specimen #	Length (mm)	Mid-Span Width (mm)	Mid-Span Thickness (mm)	Fiber Volume Fraction (%)
1	212.7	24.1	4.5	12.5
2	212.7	23.3	4.6	12.5
3	212.7	24.6	4.7	12.5
4	212.7	28.6	4.8	12.5
5	330.2	20.3	8.5	15.0
6	330.2	20.2	9.1	15.0
7	330.2	20.3	8.6	15.0
8	330.2	20.3	8.5	15.0
9	330.2	20.3	8.9	15.0

### 2.2. Test System

For the mechanical testing, a universal testing machine (type 810, MTS Systems, Eden Prairie, MN, USA) equipped with a 100 kN load cell was used to conduct three-point bend tests at a stroke rate of 1.0 mm/min. A schematic view of the three-point bending test setup is shown in Figure 1. The support span was 177.8 mm and 264.2 mm for specimens #1 to #4 and specimens #5 to #9, respectively.

A Micro-SHM AE monitoring system was employed along with the AEWIn Software (both Physical Acoustics, Princeton Junction, NJ, USA) to record and analyze the AE signals. After the initial evaluation, AE waveforms were exported to the MATLAB numeric computing environment (MathWorks, Natick, MN, USA) for further post-processing. For each test, sensors were positioned 50.8 mm to each side from the center loading location. In this study, two different types of piezoelectric sensors were used to evaluate the difference in AE response during bend testing. The piezoelectric sensor types used herein were (i) the PK15I sensor, which is a medium frequency, resonant AE sensor, and (ii) the PKWDI sensor, a wide-band frequency AE sensor (both from Physical Acoustics). Both sensor types include an integral, ultralow noise, low power, filtered, and 26 dB preamplifier. For threshold-based AE detection, the threshold was set to as low as 35 dB.

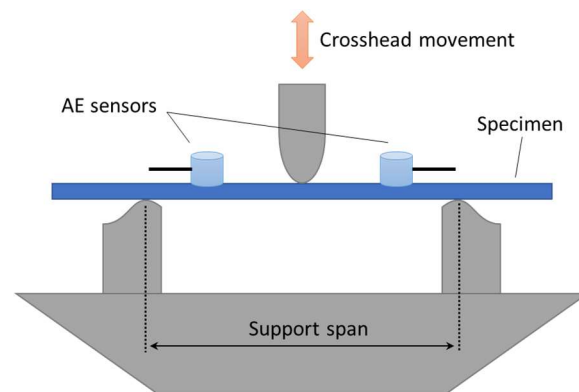


**Figure 1.** Schematic view of the three points bend test.

The sensitivity of detection and isolation of waveforms corresponding to damage in composite panels was studied using a pair of different sensors with identical timing parameters. To investigate the role of timing parameter, identical sensors, each with different timing parameters, were used in the experiments. In either configuration, labels ‘Ch1’ and ‘Ch2’ are used to indicate the two sensor channels. The following timing parameters were applied: a PDT of 50  $\mu$ sec, an HDT of 50  $\mu$ sec or 100  $\mu$ sec, and an HLT of 100  $\mu$ sec. Note that the selection of the timing parameters in AE detection depends on the specimen material properties since acoustic signals transmit and attenuate differently in different materials, for example, in composites with thermoset or thermoplastic matrices.

### 3. Results and Discussion

#### 3.1. Mechanical Properties

Three-point bend tests were conducted to determine the flexural properties of the SFRC specimens, i.e., maximum strain, maximum flexural stress, and flexural chord modulus. The selected specimen dimensions in this long beam flexure investigation yield a thickness-to-span length ratio that permits calculating ultimate flexural stress ( $\sigma$ ) and flexural strain ( $\epsilon$ ) according to Equations (1) and (2).

$$\sigma = \frac{3F_{\max}S}{2bh^2}, \quad (1)$$

$$\epsilon = \frac{6d_{\max}h}{S^2}, \quad (2)$$

where  $F_{\max}$  is the maximum load recorded at the maximum deflection of  $d_{\max}$  during the bend testing,  $S$  is the support span, and  $b$  and  $h$  are, correspondingly, the coupon mid-span width and thickness. The chord modulus was calculated based on the slope of the stress-strain curve at a 0.1% strain level. Test results are summarized in Figure 2 for the two types of specimens, i.e., with fiber volume fraction of 12.5% and 15%. As expected, the mechanical strength increased from the lower to the higher fiber volume fraction, and so did the maximum strain (~17%), maximum flexural stress (~22%), and flexural chord modulus (~8%).

The damage progress and failure modes in the SFRC laminates are presented in Figure 3 for specimens with 15% fiber volume fraction. In the early stages of deflection, small cracks on the tension plane were observed to form (highlighted by red arrows in Figure 3a). These cracks were primarily present in the resin-rich outer surface that appears highly susceptible to this type of damage during deflection. It was observed that the primary failure point initiated at one of these cracks, which did not necessary occur at the mid-span location (highlighted by a red circle in Figure 3a), that is, at the location of applied loading, which may be due to the randomness of the fiber architecture and/or slight thickness variations in these specimens made by manual processes. In some specimens, it was observed that crack propagation and the extent of delamination were not symmetric

(see Figure 3b), presumably due to the random fiber architecture. It should be noted that the term ‘delamination’ is misleading in the context of SFRC due to the absence a laminated structure. Referring to Figure 3b, ‘composite splitting’ may be a more appropriate description. Nevertheless, due to limited information on this damage type and similarities to the commonly described delamination damage mode (i.e., matrix dominated macro-scale fracturing), the notion of delamination will be maintained in the remainder of this text.

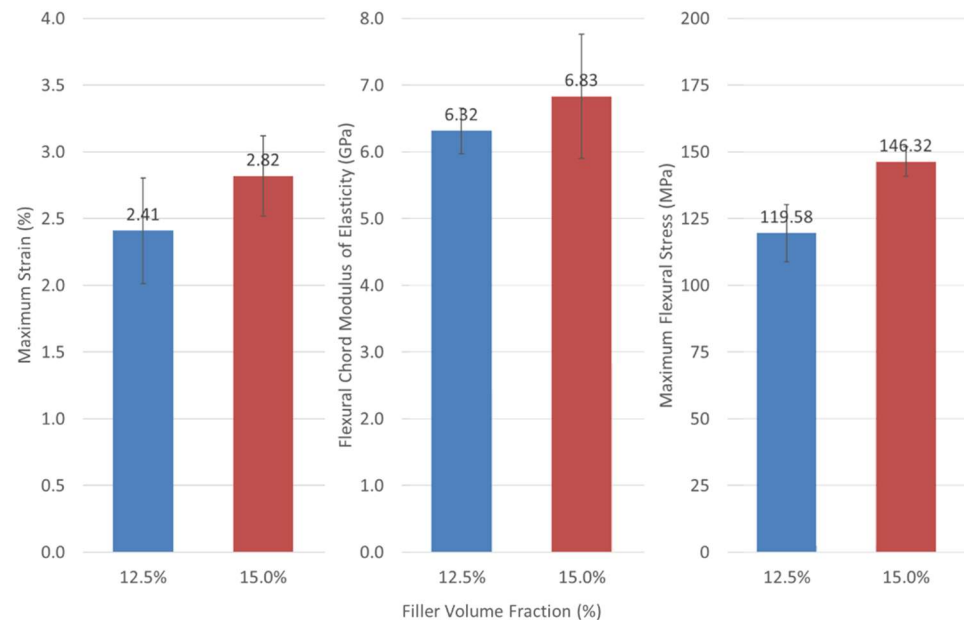


**Figure 2.** Long beam flexure properties of the SFRC panel specimens for fiber volume fractions of 12.5% and 15% (following the procedure according to ASTM D7264 [30]). Errors bars indicate plus/minus one standard deviation from the mean.

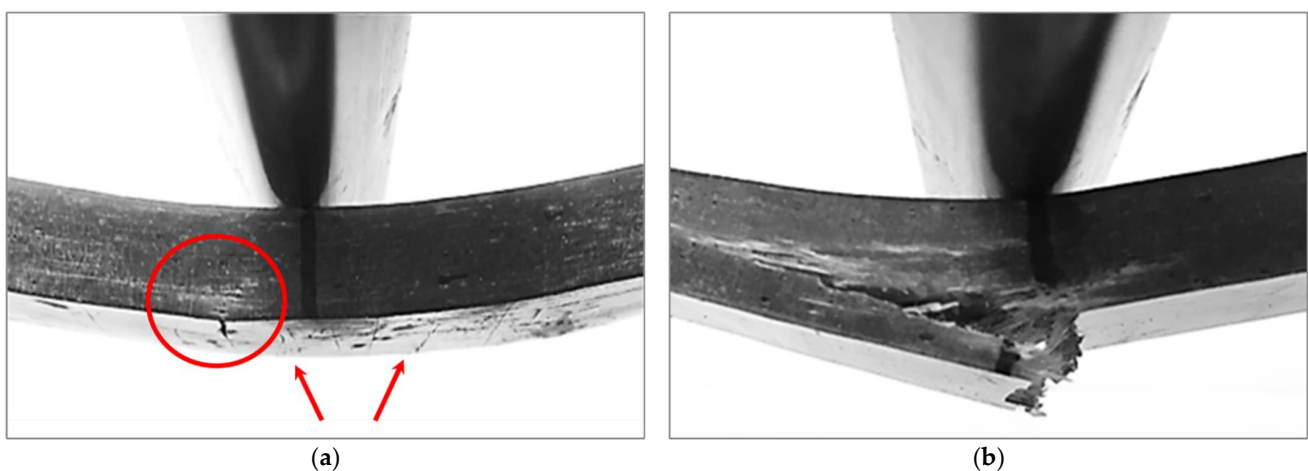


**Figure 3.** Damage progress in SFRC panel specimens with 15% fiber volume fraction; (a) crack initiation at the face under tension; (b) final failure mode.

### 3.2. Acoustic Emission—Cumulative Signal Strength

Monitoring AE activity during loading has extensively been utilized as an integrity assessment tool for FRPC. Cumulative acoustic energy (CAE) is one of the most commonly used AE features in damage progression and material characterization in composite materials. Even though the CAE can map the progress of damage under different loading scenarios, it is a relative quantity and depends on the parameters set for the testing; thus, it cannot be compared between different materials [32].

For the aforementioned reasons, the present study did not employ an approach on CAE. Alternatively, flexural stress and strain in SFRC samples during bend testing was correlated to the dynamic change in cumulative signal strength (CSS), here measured in units of pico-volt-seconds (pVs). Signal strength was calculated using the integral of the rectified voltage signal throughout the detected AE waveform. In contrast to an energy parameter approach, that is conventionally used for integrity assessment with AE, signal strength is independent of gain, which is another advantage of the employed method compared to using CAE. As mentioned above, AE monitoring was conducted with different timing parameters and using both the medium-band frequency sensors and the wide-band frequency sensors to further expand on the universality of using the CSS method.

Figure 4 depicts the CSS variation during loading correlated to flexural stress for SFRC specimens with 12.5% fiber volume fraction, with the dashed lines indicating flexural strain at certain values. In Figure 4a, the CSS data, collected using the medium-band sensors, are presented for the two different AE timing parameters (HDT: 50  $\mu$ sec (Ch1) and HDT: 100  $\mu$ sec (Ch2)). The graphs indicate a significant jump (two orders of magnitude and more) in CSS at a flexural strain of 1.9%, indicating a strong increase in the number of AE hits and strength of the detected signals. After the jump, an increased slope of the CSS graph is indicative of higher damage accumulation and progress in the later stage of testing approaching sample failure. Despite using different AE timing parameters, both sensors detected the jump in CSS at the same flexural strain (1.9%). It should be noted that the AE timing parameter selection in a threshold-based AE hit detection technique does not guarantee perfect signal waveform detection. However, an effort should be placed to tune them by checking the signal waveforms after AE recording. Here, the study showcased that a modest parameter difference does not affect the overall AE performance for integrity assessment.

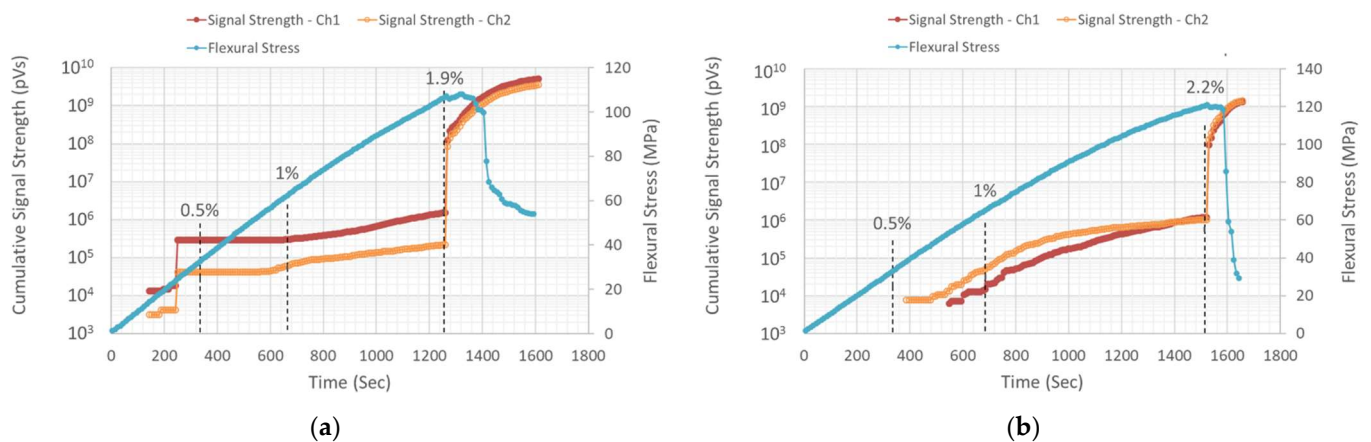


**Figure 4.** CSS (left axis) and flexural stress (right axis) over time for SFRC specimens with 12.5% fiber volume fraction, using (a) medium-band frequency sensors with different AE timing parameters, and (b) using a medium-band and wide-band frequency sensor with the same AE timing parameters. Dash lines indicate flexural strains.

In Figure 4b, CSS data are compared for a test using the medium-band (Ch2) and wide-band (Ch1) sensors, both having the same AE timing parameters for AE monitoring (HDT: 100  $\mu$ sec). Despite the difference in signals detected in the early stages of coupon deflection, both sensors indicated a significant jump at 2.2% flexural strain. A micro-cracking damage mode is expected to dominate the early stage of bending (<1% flexural strain), which is reported to typically have lower signal strength and peak frequency values (see Table 1). Therefore, the higher sensitivity of the medium-band sensor at lower frequency ranges leads to detecting more AE hits at these frequency levels.

In Figure 5a, CSS data is correlated to the flexural stress and strain level in two samples with a 15% fiber volume fraction. The medium-band sensors were again used in these tests

with two different AE timing parameters (HDT: 50  $\mu$ sec (Ch1) and HDT: 100  $\mu$ sec (Ch2)). Similar to the trend observed in Figure 4a, there is a shift along the ordinate in the graph due to more hits being detected for the lower HDT setting. Despite this difference, both timing parameter settings detected a significant jump in CSS at the same flexural strain. Referring to Figure 5b, characteristic features (i.e., jumps) are indicated using in the CSS graphs, when both the medium-band (Ch1) and wide-band sensor (Ch2) were used with the same AE timing parameters, which supports the observation made from Figure 4b for the SFRC specimen with 12.5% fiber volume fraction.

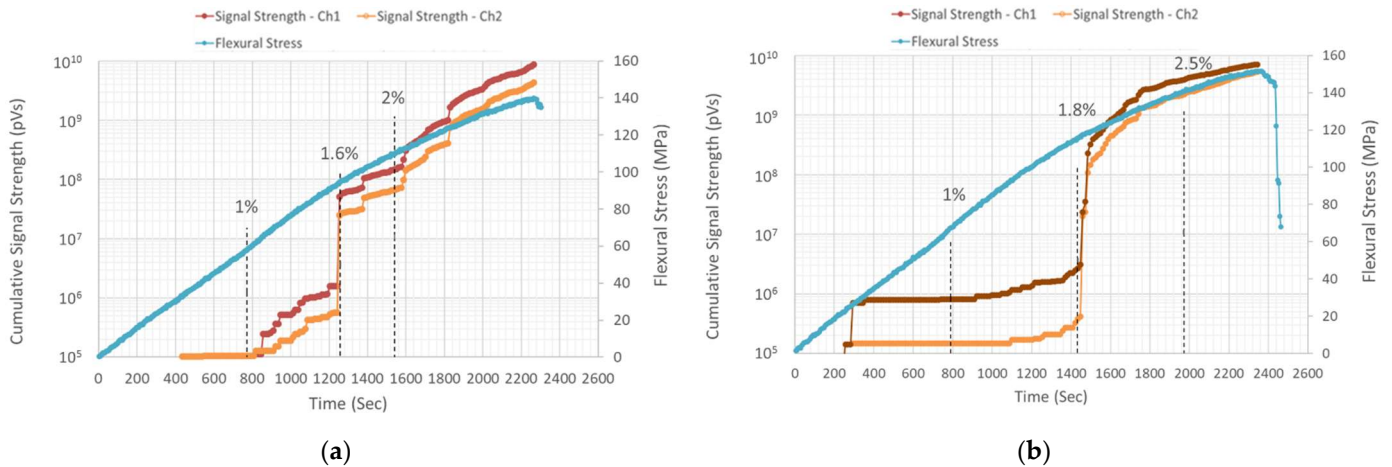


**Figure 5.** CSS (left axis) and flexural stress (right axis) over time for SFRC specimens with 15.0% fiber volume fraction, using (a) medium-band frequency sensors with different AE timing parameters, and (b) using a medium-band and wide-band frequency sensor with the same AE timing parameters. Dash lines indicate flexural strains.

For the full sets of specimens (as per Table 2), a reduction of the average flexural strain values that coincide with the characteristic jump in the CSS curves (as per Figures 4 and 5) is depicted in Figure 6. This graph suggests that, by means of AE recordings, a strain damage threshold can successfully be defined for each type of composite panel. The employed methodology is not only sensitive to the fiber volume content, as shown here, but also to fiber and matrix properties, which, however, is outside the scope of this paper. Consequently, the present analysis of AE recordings is shown to be a feasible and expedient means for quality control and integrity assessment of SFRC panels.

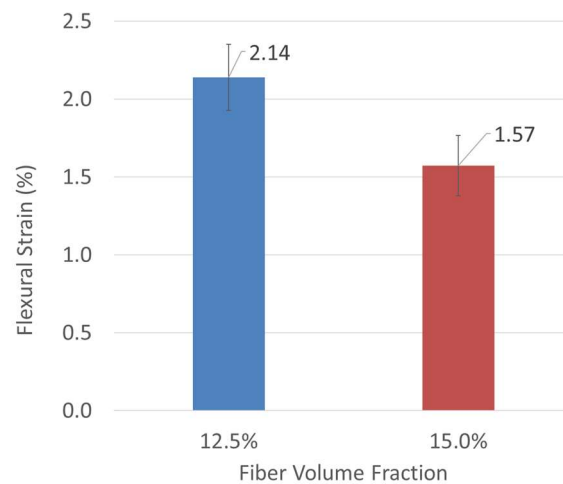


**Figure 6.** Comparing flexural strain thresholds derived from AE data in SFRC panel coupons with different fiber volume fractions.

### 3.3. Acoustic Emission—Waveform Features

This section explores in greater detail the recorded AE hits using different waveform features, including amplitude, duration, peak frequency, and signal strength. Studying the AE hits distribution considering multiple signal features facilitates identifying the coherence and similarity in AE response within test samples. Figure 7 presents the AE hits that were recorded for a sample with 12.5% fiber volume fraction, by means of the medium-band sensors, from the start of a flexural test until the sample reached its maximum strength. As shown in Figure 7a, the majority of hits have durations of less than 1000  $\mu\text{sec}$ . Scatter plots in Figure 7b,c, for the maximum signal amplitude and signal strength versus signal peak frequency, respectively, exhibit clusters of hits that can be identified based on peak frequency. A graph with CSS and cumulative hits versus peak frequency is presented in Figure 7e. Noticeable jumps in this graph demarcate considerable AE activity with similar peak frequencies, whereas plateaus indicate either AE hits with insignificant signal strength or the absence of AE hits between clusters. A first jump occurs roughly at a peak frequency of 150 kHz, and a second at 250 kHz. The clustering of hits at these frequencies is also clearly visible in Figure 7d. This graph also indicates that AE hits with a peak frequency above 300 kHz were only recorded close to the sample reaching its maximum flexural strength.

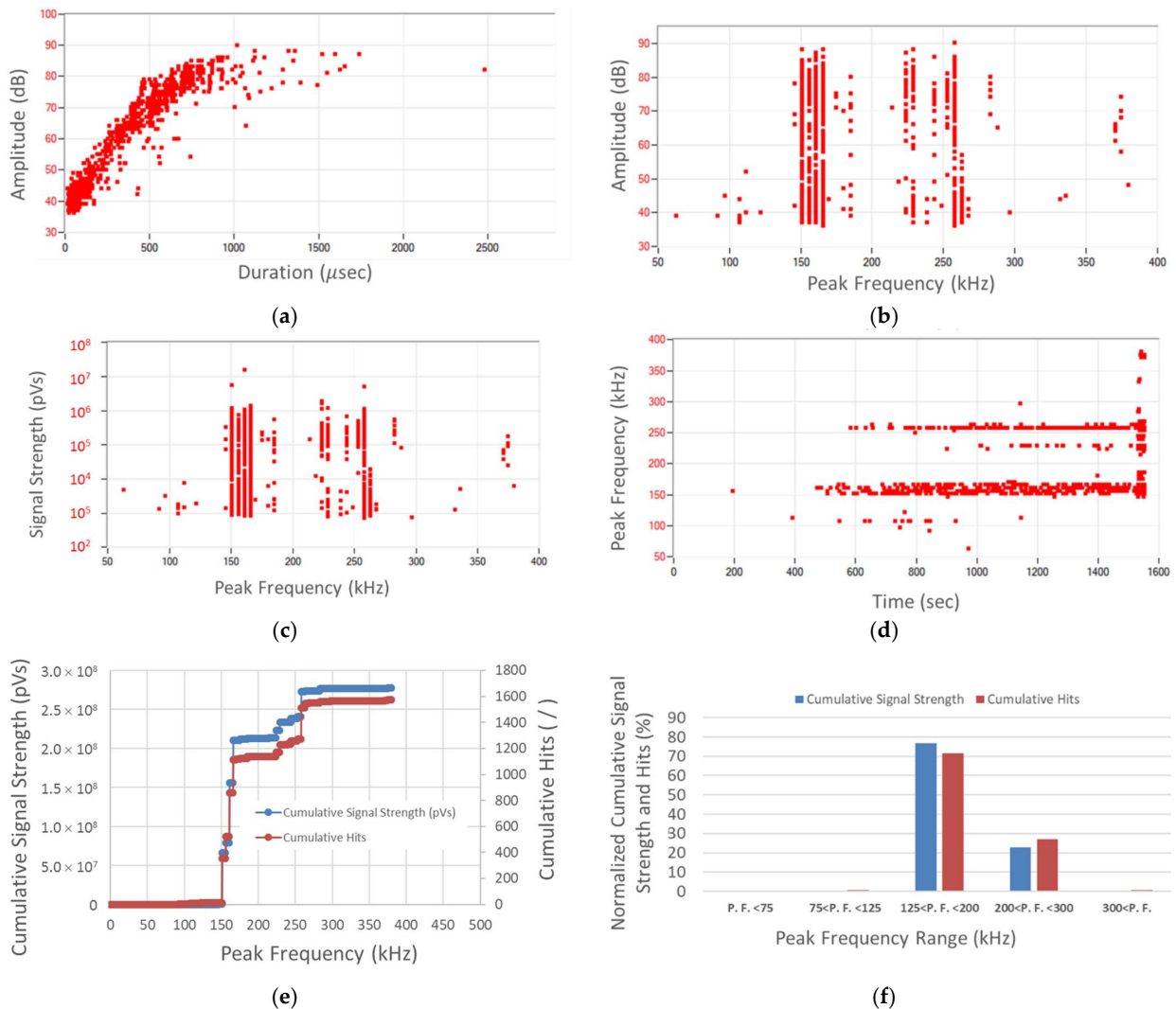


**Figure 7.** (a) AE hits distribution based on amplitude versus duration, (b) amplitude versus peak frequency, (c) signal strength versus peak frequency, and (d) peak frequency versus time; (e) CSS and cumulative hits versus peak frequency, and (f) normalized CSS and cumulative hits for different peak frequency ranges.

Referring to Table 1, where FRC damage modes are identified in terms of frequency range as found in the technical literature, matrix cracking was reported to produce signals within the lowest peak frequency range, whereas fiber failure is indicated by signals with the highest peak frequencies. In Figure 7f, AE signals in terms of normalized CSS are binned using five peak frequency ranges, according to a similar approach employed in Reference [18]: (i) less than 75 kHz, (ii) 75 kHz to 125 kHz, (iii) 125 kHz to 200 kHz, (iv) 200 kHz to 300 kHz, and (v) greater than 300 kHz. As shown in this graph, more than 70% of AE hits fall into the 125 kHz to 200 kHz peak frequency range, and about 28% into the 200 kHz to 300kHz range. Considering the values presented in Table 1, it can be speculated that these ranges correlate with matrix micro-cracking and fiber-matrix debonding, and delamination and fiber breakage, respectively.

The sensitivity of AE hits and the corresponding CSS to the AE timing parameter setting was examined by using the two different sets of timing parameters, i.e., HDT: 50  $\mu$ sec versus HDT: 100  $\mu$ sec. Results for these two cases are contrasted in Figure 8 for a sample with 12.5%, where CSS data and hits are plotted versus peak frequency. Notably, both timing settings resulted in jumps in the CSS and hits at practically identical peak frequency of  $\sim$ 150 kHz and  $\sim$ 250 kHz, as shown in Figure 8(a-i,b-i). For the case of HDT: 50  $\mu$ sec, in Figure 8(a-ii), about 80% of detected hits have a peak frequency between 125 kHz and 200 kHz, whereas, in the case of HDT: 100  $\mu$ sec, in Figure 8(b-ii), the majority of hits falls into the range of 200 kHz to 300 kHz. Hence, identifying the extent of damage is found to be sensitive to the AE timing parameter selection, even though integrity assessment of the composite panels using CSS is ascertained to have low sensitivity to the AE timing parameter (as indicated by Figures 4a and 5a).

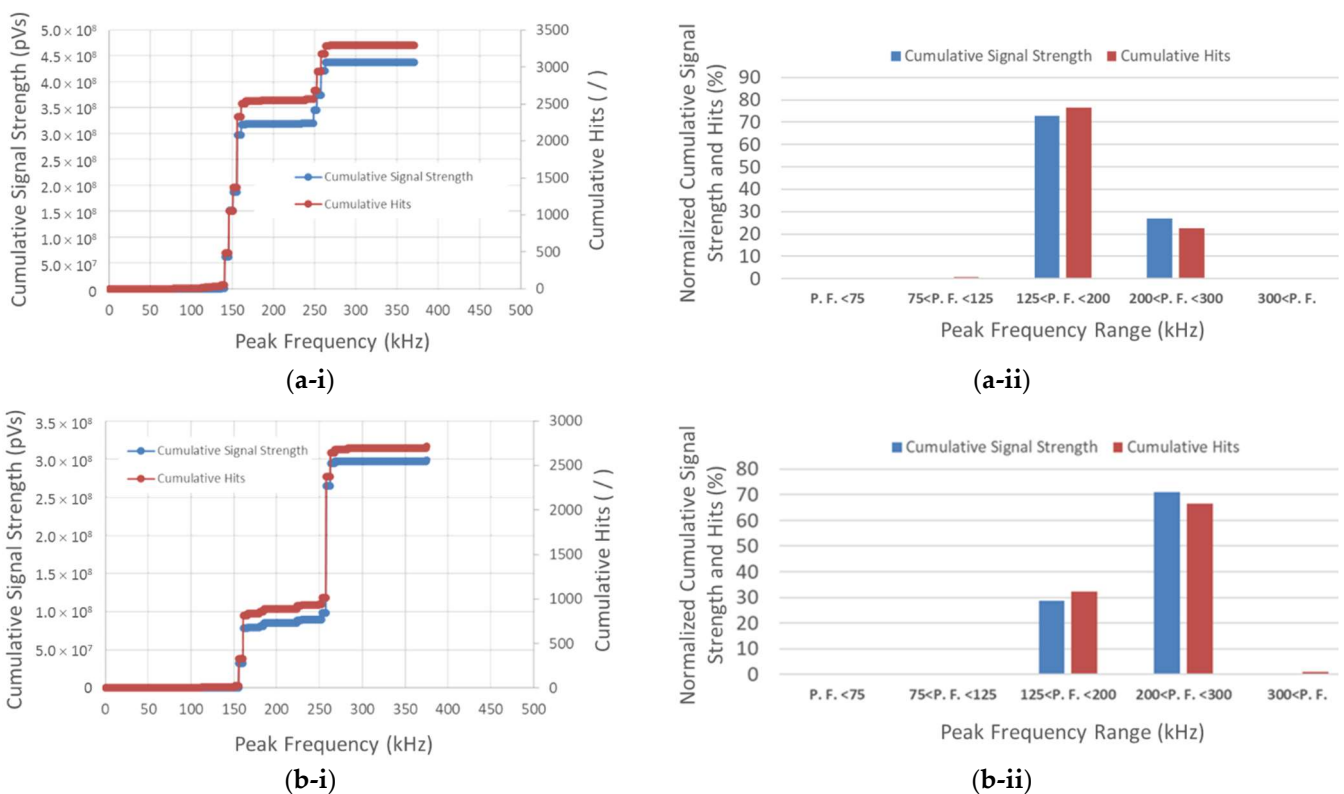


**Figure 8.** AE data for timing parameters of (a) HDT: 50  $\mu$ sec and (b) HDT: 100  $\mu$ sec, showing (i) CSS and cumulative hits versus peak frequency, and (ii) normalized CSS and cumulative hits for different peak frequency ranges.

In Figure 9, AE hits are compared in terms of maximum amplitude, peak frequency, and duration for samples with fiber volume fractions of (a) 12.5% and (b) 15%. In these

tests, medium-band sensors with AE timing parameters of HDT: 50  $\mu\text{sec}$  and HLT: 100  $\mu\text{sec}$  were used. In samples with lower fiber volume fraction (that were also thinner; see dimensions reported in Table 2), the number of detected AE hits was less than for samples with higher fiber volume fraction. In general, a lower number of AE hits simplifies the visual identification of clusters based on peak frequency in Figure 9(a-ii) as compared to the sample with more AE hits in Figure 9(b-ii). It can further be ascertained that the larger relative fiber content, the larger sample dimension, or both resulted in more hits in peak frequency ranges that appear to be associated with debonding and fiber pull-out (125 kHz to 200 kHz). At this juncture, it is worth emphasizing the efficacy of the chosen AE analysis method, considering that the SFRC samples with randomly-oriented short fibers are subject to more complex internal stress distributions as compared to composite systems with unidirectional fiber plies or samples with certain ply stacking.

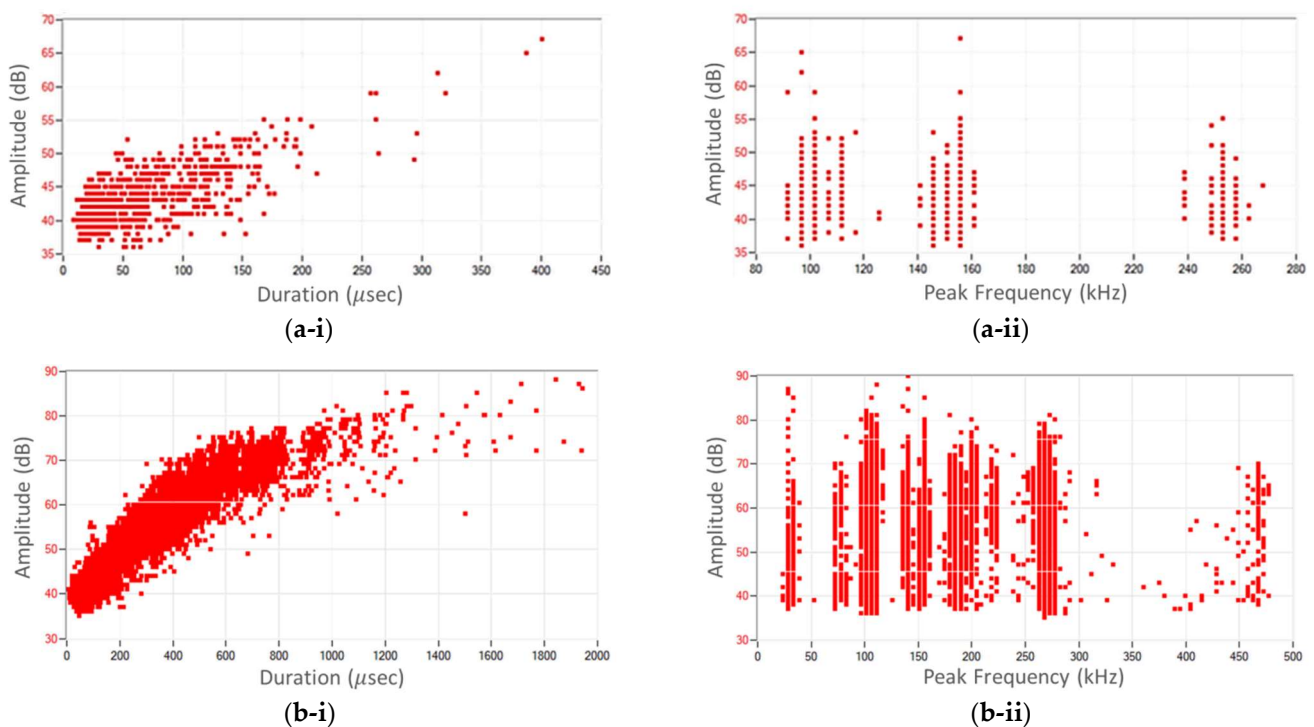


**Figure 9.** AE hits distribution for samples with fiber volume fraction of (a) 12.5% and (b) 15%, based on (i) amplitude versus duration, and (ii) amplitude versus peak frequency.

### 3.4. Acoustic Emission—Peak Frequency Classification

Figure 10a,b depict CSS and cumulative hits versus peak frequency of AE waveforms for samples with fiber volume fractions of 12.5% and 15%, respectively. Comparing Figure 10(a-i,b-i), it is seen that, in the sample with the higher fiber volume fraction, CSS is about three orders of magnitude higher than for the sample with the lower relative fiber content. Despite the difference in relative fiber content, both types of samples exhibit clustering of AE hits in three distinct peak frequency ranges, which are postulated to concur with matrix cracking (less than 125 kHz), fiber debonding (125 kHz to 200 kHz), and delamination and fiber breakage (greater than 200 kHz).

While the bar charts in Figure 10(a-ii,b-ii) expediently identify the overall signal accumulation within specific peak frequency ranges, temporal information is lacking about the dynamics of characteristic peak frequencies. The latter information is provided for samples with a fiber volume fraction of 12.5% and 15%, by the graphs in Figure 11a,b, respectively, where CSS data is separated for each of the five frequency ranges employed previously. These graphs, thus, allow tracking the progression of damage modes over time. Two scenarios have been observed herein in terms of CSS dynamics: (1) a gradual increase

with a significant jump at the test mid-time (Figure 11b) and (2) a steady increase with a significant jump close to sample failure (Figure 11a).

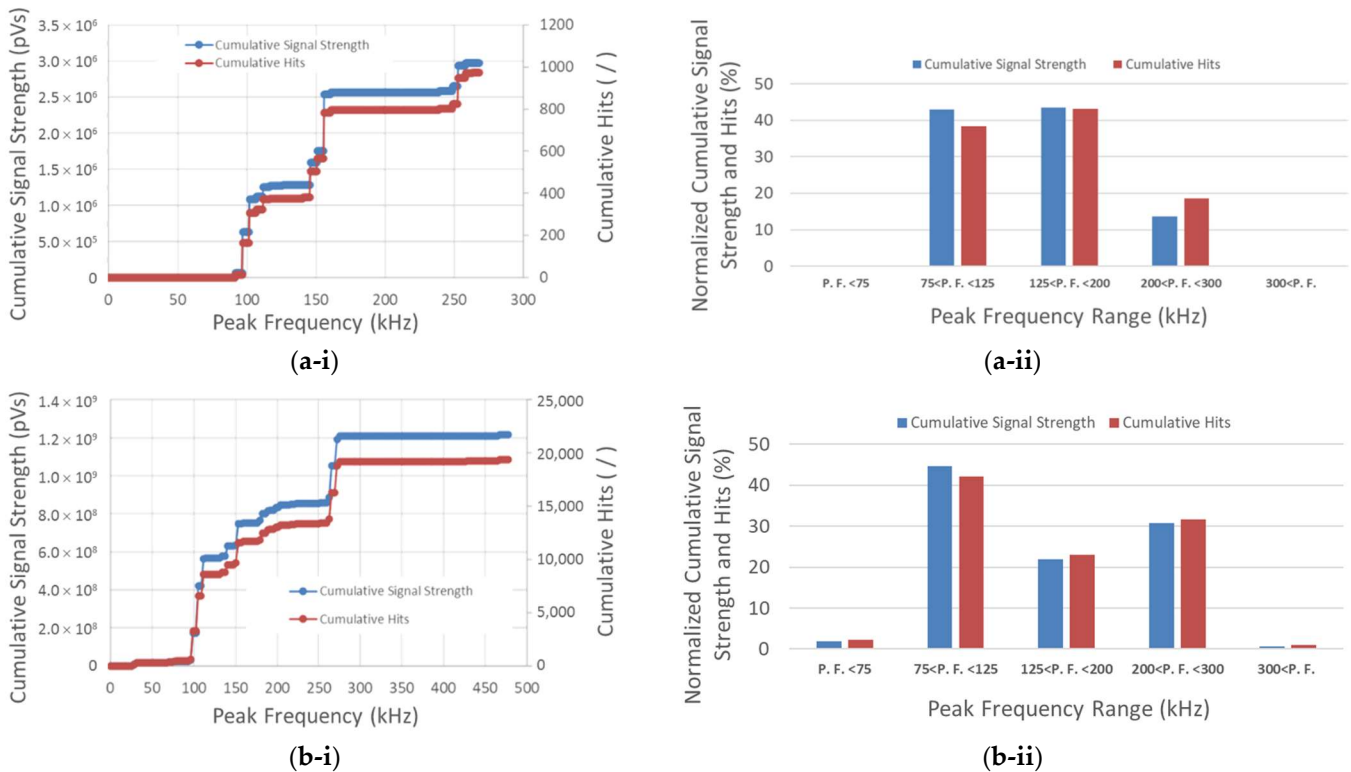


**Figure 10.** AE data for samples with fiber volume fraction of (a) 12.5% and (b) 15%, showing (i) CSS and cumulative hits versus peak frequency, and (ii) normalized CSS and cumulative hits for different peak frequency ranges.

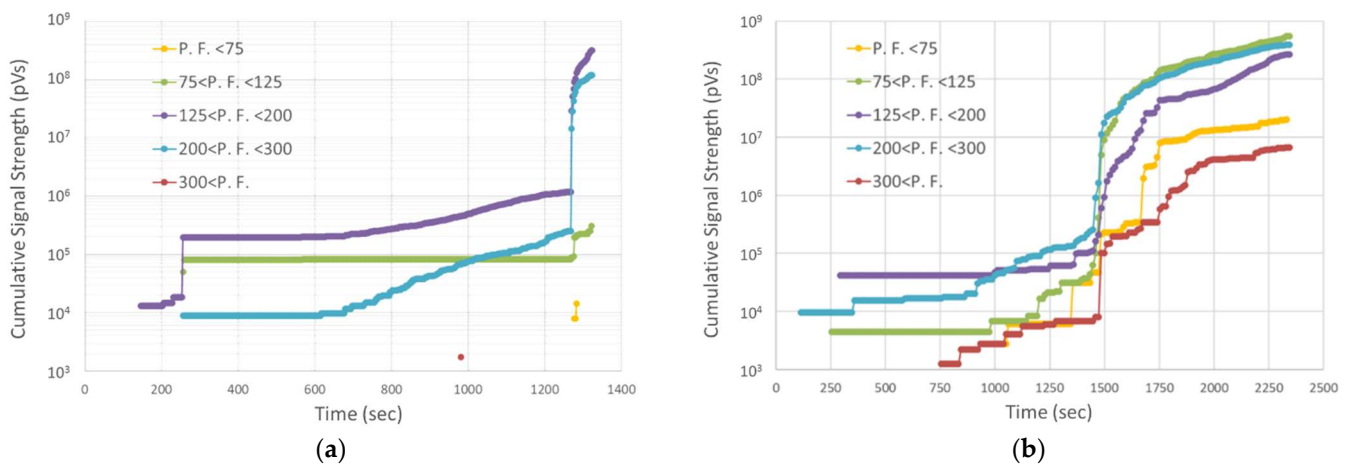


**Figure 11.** Evolution of CSS for different peak frequency ranges, in samples with a fiber volume fraction of (a) 12.5% and (b) 15%.

For scenario (1), significant jumps are apparent in the CSS curves for all specified peak frequency ranges (Figure 11b). In general, an increase in a CSS curve indicates an accumulation of AE hits, whereas a plateau represents a lack of hit detections. In the early stage of the flexural test, AE hits with peak frequencies in the range of 200 kHz to 300 kHz occur predominantly, presumably due to delamination damage, compared to the other peak frequency ranges. Significant AE activity can also be ascertained for the

peak frequency ranges of 75 kHz to 125 kHz and 125 kHz to 200 kHz, which are likely associated with matrix micro-cracking and fiber-matrix debonding, respectively. On the other hand, lower CSS magnitudes can be ascertained for AE hits with peak frequencies below 75 kHz and above 300 kHz, which likely occurs for two reasons. First, AE hits with peak frequencies below 75 kHz would be associated with matrix micro-cracking, which typically produces low signal amplitude and duration and, thus, reduced signal strength. Second, a low quantity of AE hits also results in low CSS magnitude, which can reasonably be assumed for fiber breakage in this case.

For scenario (2), note that a thin specimen was used that is, therefore, less rigid than the specimen type in scenario (1). The primary CSS contributors are AE hits in the ranges of 125 kHz to 200 kHz and 200 kHz to 300 kHz, corresponding presumably to fiber-matrix debonding and delamination damage, respectively. The AE hits cause CSS magnitudes to gradually increase until a sudden jump that occurs late in the specimen life (near maximum flexural strength). On the other hand, AE hits with peak frequencies above 300 kHz did practically not occur, the latter indicating the near absence of fiber breakage. In terms of matrix micro-cracking, it remains uncertain if a lack of AE hits with peak frequencies below 75 kHz is truly indicative of this damage mode being absent, or if this damage mode produces AE hits also in the 75 kHz to 125 kHz range. Therefore, it stands to reason that additional research is required to clearly identify the peak frequency ranges for specific damage modes in an SFRC material, which may require test configurations other than flexural testing.

### 3.5. Acoustic Emission—Other AE Features

Other commonly used AE features to correlated the AE response to the damage progress in addition to the peak amplitude and the peak frequency are weighted peak frequency [33–37], rise time [37,38], and the RA value [38,39]. This section explores the damage progression of SFRCs based on these three AE features.

The weighted peak frequency (WPF) is defined as

$$PF_W = \sqrt{F_c \times F_p}, \quad (3)$$

where  $F_c$  is the frequency centroid, and  $F_p$  is the peak frequency of the AE hit. The integration of the frequency centroid to the peak frequency using the WPF definition was shown to provide more significance to the power spectrum than the peak frequency alone [33–37]. AE analysis of glass/carbon fiber hybrid composites showed that four weighted peak frequency ranges of 50–160 kHz, 150–300 kHz, 300–400 kHz, and 400–600 kHz could be attributed to four different failure types occurring in laminates, i.e., matrix cracking, interface failure, fiber pull out, and fiber breakage, respectively [36].

In Figure 12, AE hits are presented based on the peak amplitude, duration, and WPF of waveforms for two different SFRC samples (S7 and S8), with 15% fiber volume fraction, using the medium-band frequency sensors. For both specimens, AE hits appear to be clustered into three classes. However, these classes do not coincide with those reported in Reference [36]. The AE hits distributions based on WPF suggest using this AE feature in multi-variable AE data clustering studies for SFRCs.

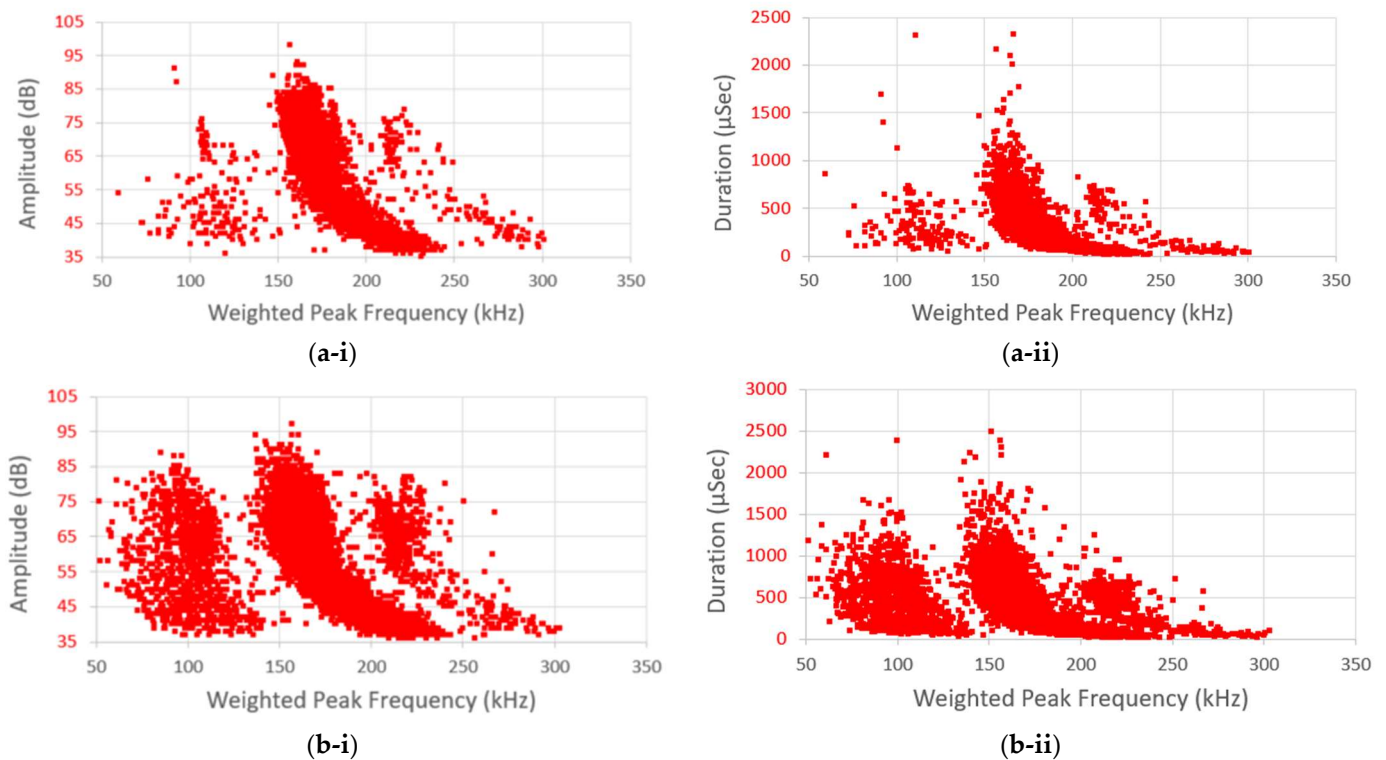


**Figure 12.** AE hits distribution based on (i) peak amplitude, (ii) duration, and weighted peak frequency for samples (a) S7 and (b) S8 with 15% fiber volume fraction.

Besides the aforementioned AE features, a popular AE parameter is the rise time (time between a first threshold crossing and the peak amplitude). Rise time has been widely used in multi-variable AE clustering studies [16,17,23,24,33,37,38]. In Reference [38], rise time was tracked at different stress levels at static loading in CFRP to identify and differentiate between failure modes. It was concluded that a low rise time ( $<100 \mu\text{sec}$ ) represents matrix cracking, whereas a higher rise time ( $>100 \mu\text{sec}$ ) represents shear debonding and interlaminar delamination. In Figure 13, AE data for the same specimens (S7 and S8) are presented based on the peak amplitude and rise time of the recorded AE hits, along with the distribution of AE hits rise time over time. It is evident that the bulk of the recorded AE hits have rise times of less than  $100 \mu\text{sec}$ , while the majority of AE hits with rise times greater than  $100 \mu\text{sec}$  were recorded close to the ultimate flexure strength of the SFRCs, which confirms the correlation between the shear debonding failure mode and AE hits with rise times greater than  $100 \mu\text{sec}$ .

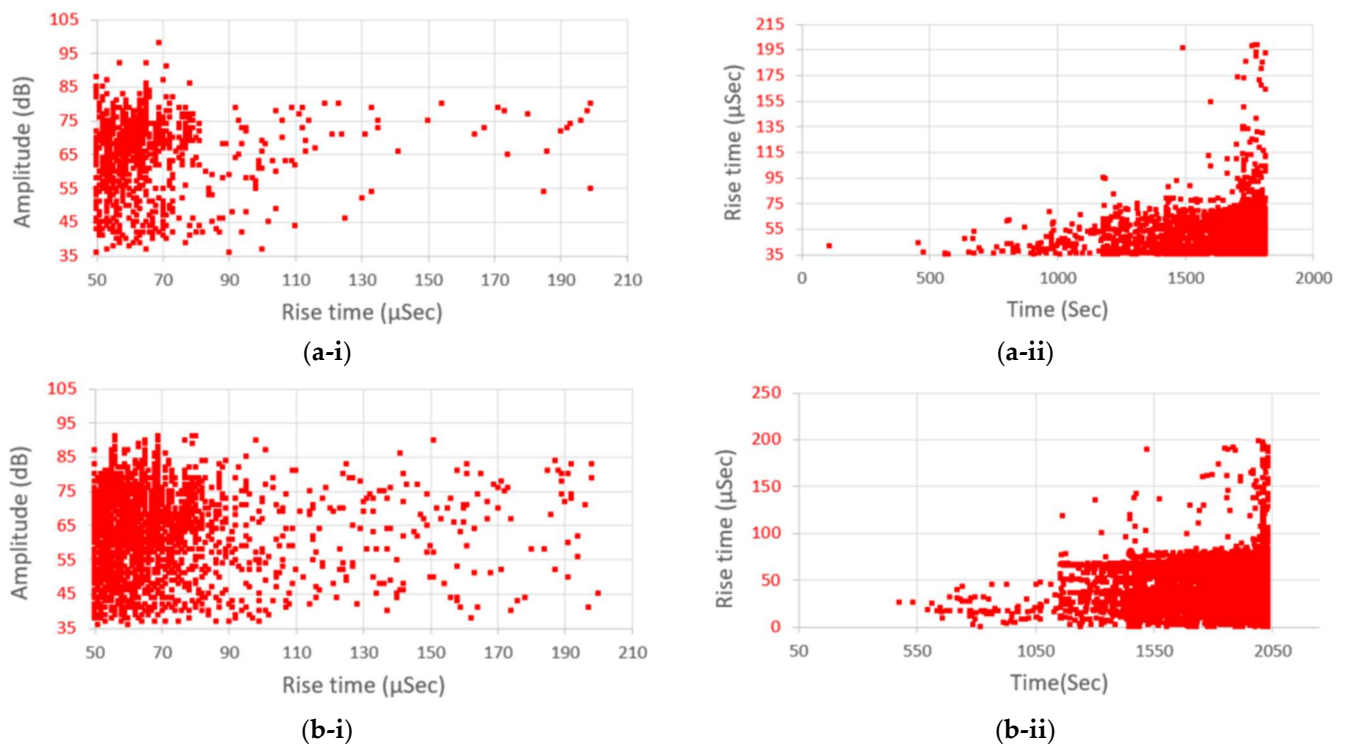


**Figure 13.** AE hits distribution based on (i) amplitude, (ii) rise time, and time for samples (a) S7 and (b) S8 samples with 15% fiber volume fraction.

Another efficient method of using amplitude and rise time is suggested in References [38,39], to characterize tensile and shearing events within the composites under loading. These works introduced the RA value (as mentioned above, defined as the ratio of rise time to the peak amplitude of an AE hit). It was concluded that the damage modes induced by tension produces AE hits with lower rise time and higher peak amplitude, whereas shearing within the material emits acoustic waves with higher rise time and lower peak amplitude. In the original definition of the RA value, the peak amplitude is expressed in volts (V). The present analysis takes a modified approach, in which the peak amplitude is represented in decibel (dB). Considering the 26 dB preamplifier gain applied in the AE sensors used in this study, the amplitude is given by,

$$Amp.(V) = 20 \times 10^{-6} \left[ 10^{\left( \frac{[Amp.(dB)+26]}{20} \right)} \right]. \tag{4}$$

In Figure 14, RA and CRA values for AE hits are presented and compared using the units of V and dB for the peak amplitude. For both RA definitions, an increase in RA value stands for reaching the peak amplitude more rapidly. In Figure 14(a-i,a-ii), the RA values recorded for AE hits during flexural testing are presented. Presumably, damage at the early stage of flexural testing is mostly due to matrix cracking as a result of tension on the outer specimen face. Correlating this damage mode to the values for the RA parameter in each definition serves to characterize damage progression based on the RA value. Plotting the RA values in logarithmic scale indicates similarities in RA variation over time for both definitions. Notably, RA values with some of the lowest and highest recorded values emerge close to the ultimate flexural strength, which may be indicative of major damage events. Nevertheless, compared to unidirectional and/or laminated reinforced specimens the damage progress in SFRC specimens is complex due to the random fiber orientation. Therefore, further detailed studies with well-defined fiber orientations are required to match damage modes to RA values. Next, referring to Figure 14b, RA data are presented in the form of CRA for both RA definitions. The CRA data is plotted in log-scale to help

identify any significant jumps in CRA data during flexural loading. While the CRA data using peak amplitude in unit V exhibited a gradual increase over time, the CRA data based on peak amplitude in unit dB revealed two such jumps (highlighted by ellipses in the figure). The occurrence of these jumps requires further investigation, however.

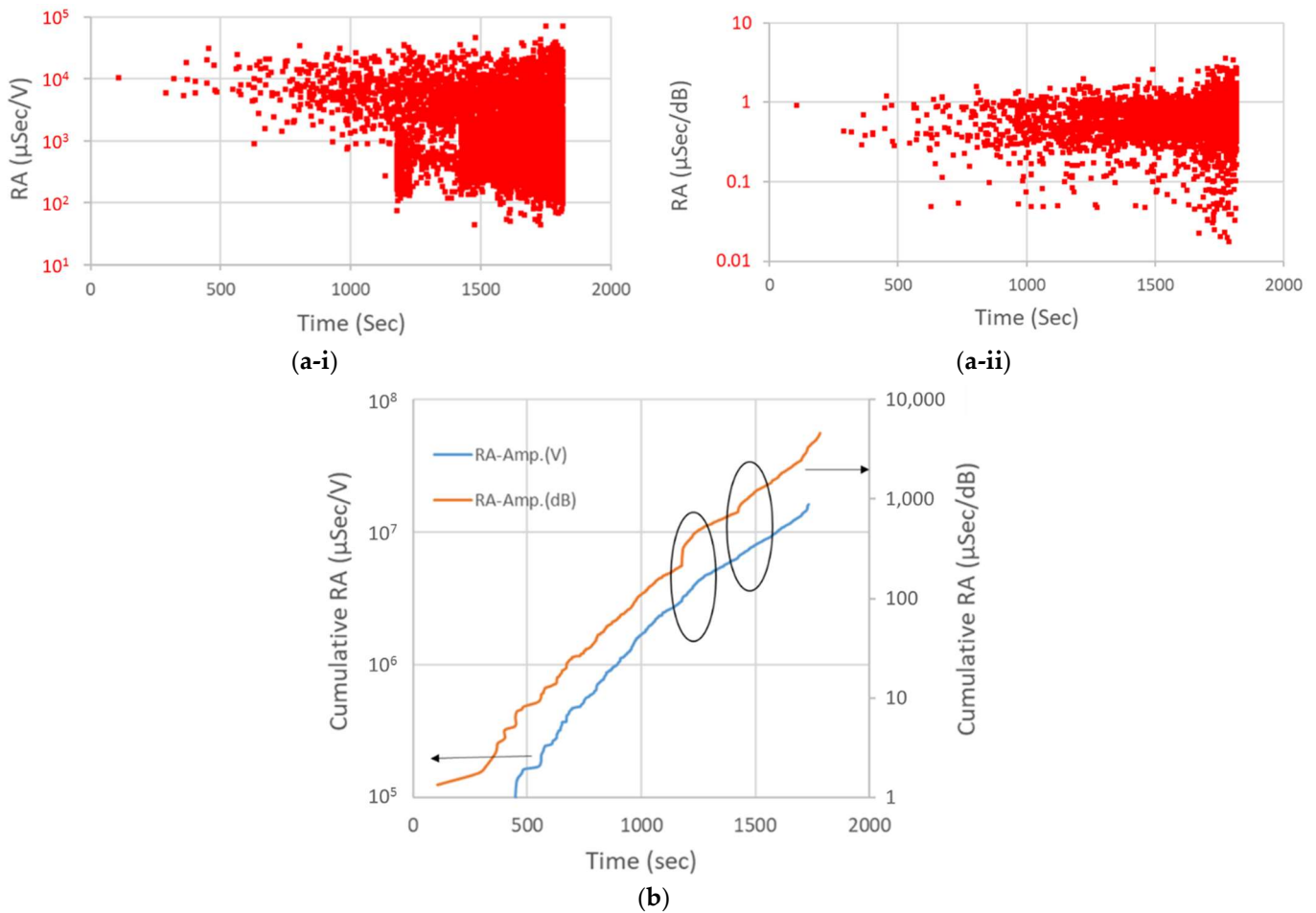


**Figure 14.** Comparing (a) RA values for recorded AE hits using (i)  $\mu\text{Sec/V}$  definition and (ii)  $\mu\text{Sec/dB}$  definition and (b) the CRA progression during the flexural loading, using a peak amplitude representation based on volts (V) and decibel (dB), for sample S7 with 15% fiber volume fraction.

In Figure 15a, RA values are presented based on the proposed RA definition (i.e., using unit dB) for AE hits recorded during flexural loading of specimen S7 with respect to time, duration, and peak amplitude. Presumably, AE hits with RA values less than unity are associated with tension damage modes in the SFRC, such as matrix cracking and fiber breakage, whereas AE hits with RA values greater than unity are the result of fiber matrix debonding and delamination. In the early stages of flexural testing, AE hits have lower RA values, whereas, in late-stage testing, close to the ultimate flexural strength, RA values with considerably higher magnitude are present. The preceding presumption is justified by the observation that AE hits with RA values less than unity are associated with low rise time and high duration and, thus, fiber breakage. Figure 15b further explores the RA approach by correlating CRA and CSS data. From Section 3.2, recall that a significant jump in the CSS data indicated the initiation of major damage progression in SFRCs. Locations of jumps in the CRA curve are highlighted using arrows in Figure 15b. Notably, these locations coincide with jumps in the CSS graph. Again, employing a logarithmic scale in the CRA and CSS plots aids in identifying the jumps.

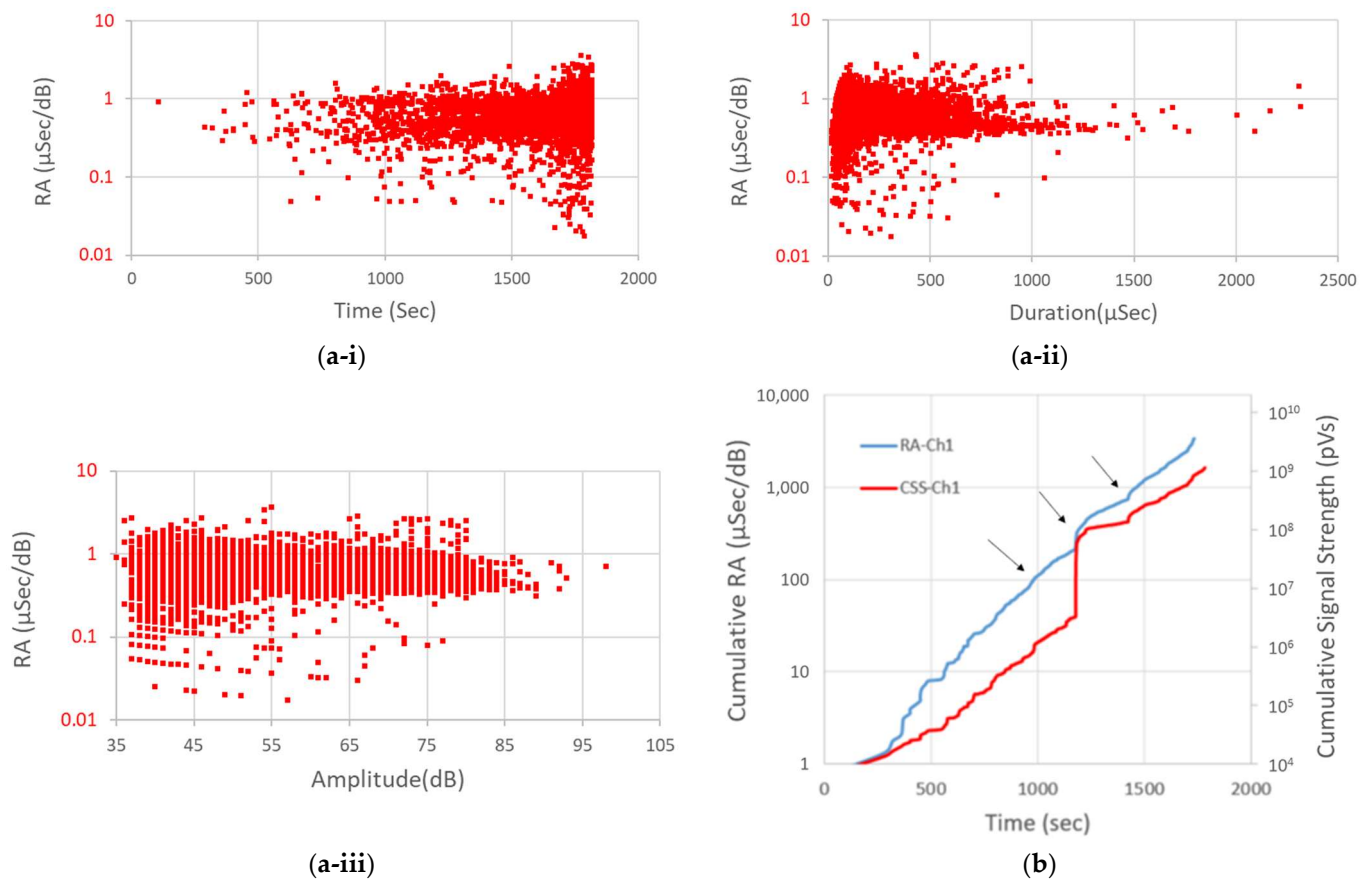


**Figure 15.** AE hits distribution based on RA value versus (a-i) time, (a-ii) duration, and (a-iii) amplitude and (b) correlating CRA value to the CSS during the flexural loading of S7 (medium-band frequency sensor).

Finally, in Figure 16, CRA and CSS data are compared for different specimens using different type of AE sensors. Remarkably, significant jumps in CRA curves coincide with significant jumps in the CSS data for different specimens, and regardless of sensor type (medium-band or wide-band). Specifically, Figure 16(a-i,a-ii), contrast recorded CRA and CSS data for different sensor types, revealing that, despite the differences in CRA and CSS data over the course of specimen loading, it is possible to use either sensor type to (i) identify the initiation of major damage and (ii) characterize the damage progression with respect to the failure mode using the variation in slope of CRA curves.

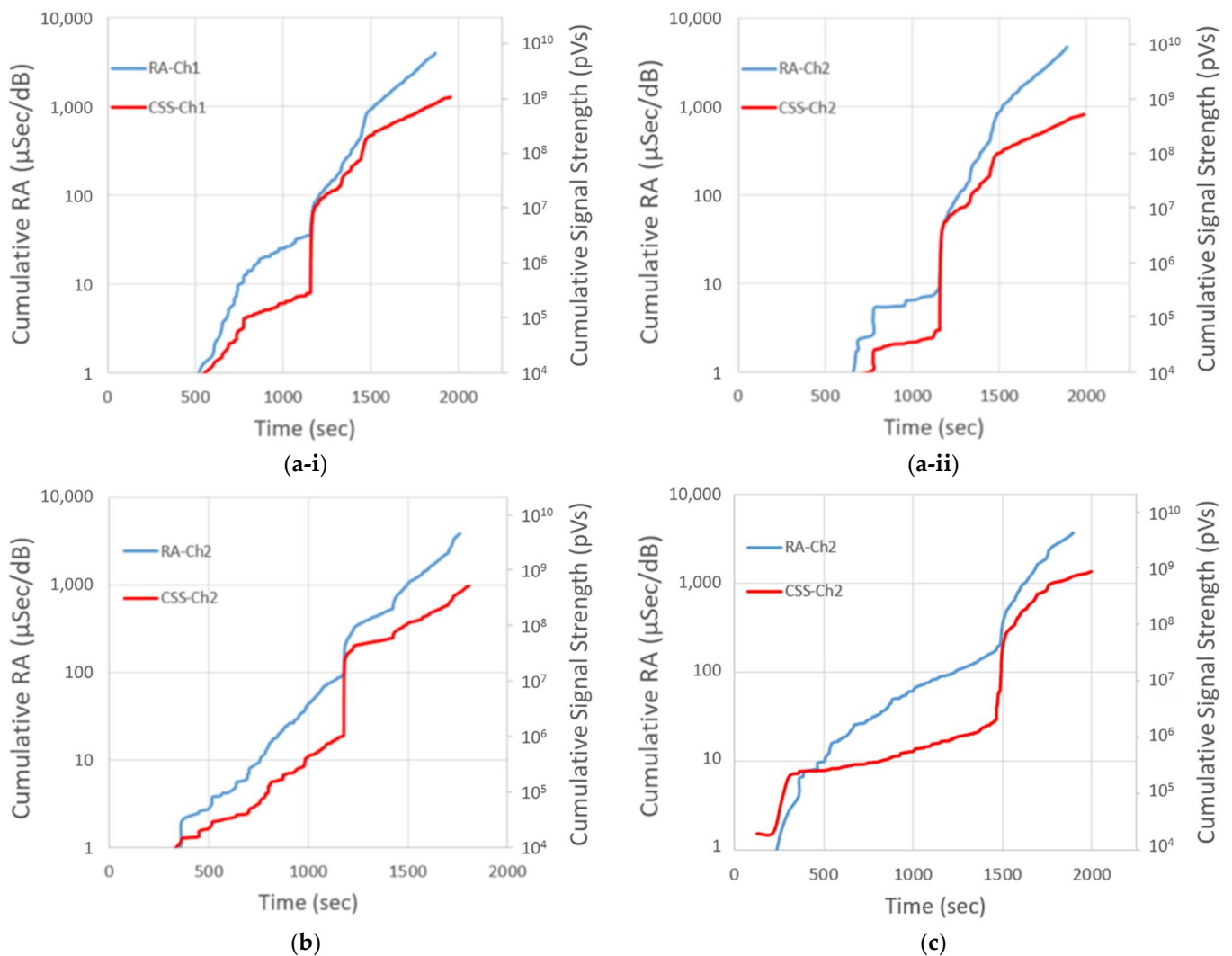


**Figure 16.** CRA and CSS data for flexural loading of (a) specimen S8 using (i) a medium-band and (ii) wide-band frequency sensor; (b) specimens S7 and (c) S9 using wide-band frequency sensors.

#### 4. Conclusions

In this study, acoustic emission (AE) was employed as a non-destructive tool for integrity assessment in short glass fiber-reinforced composite (SFRC) panels. This class of composite materials has received only limited attention by researchers in the context of AE analysis in the past. Through three-point bend testing, the flexural properties, including flexural chord modulus, and maximum flexural stress and strain, were determined for coupon samples with different fiber volume fractions and dimensions. AE detection was conducted during bend testing, revealing the flexural damage progress for composite panel coupons. AE data was detected using two different types of piezoresistive transducers, i.e., medium-band and wide-band frequency sensors, and different AE timing parameters. This study demonstrated that the employed CSS and CRA approaches facilitate integrity assessment of such panel structures as significant jumps in CSS and CRA curves reliably indicate damage thresholds in terms of strain during flexural testing.

While the present CSS-based integrity assessment approach was shown to be practically independent to the applied sensor type (medium-band versus wide-band), it was also found to be somewhat sensitive to the set AE timing parameters. Still, significant jumps (more than two orders of magnitude) in CSS data can be used as a reliable quantitative criterion for integrity assessment as it was not sensitive to sensor type and AE timing parameters.

This study attempted a damage modes identification based on peak frequency distributions and characteristic frequency bands as defined in the technical literature. CSS results were found to form clusters for certain peak frequency bands, suggesting an association with distinct failure mechanism. AE waveform clustering suggests that fiber-matrix debonding, delamination and fiber breakage significantly contributed to specimen failure. However, because the short glass fibers composite panels used in this study feature randomly distributed and oriented reinforcement elements, the typical trend in damage progression reported in the technical literature for laminated composites, i.e., matrix cracking, followed by fiber debonding and delamination and, finally, fiber breakage, could not be confirmed in the present study. Strictly speaking, delamination does not occur in SFRC due to the absence of a laminated structure. Still, it is conceivable that a comparable damage mode, observed and termed herein as matrix splitting, may produce AE signals similar to a delamination damage mode due to the characteristic of forming macro matrix fractures.

The redefinition of the RA parameter (in unit decibel, rather than volts) showed to be effective in integrity assessment of SFRCs as significant jumps in CRA curves aligned with CSS data. Nevertheless, in order to reliably correlate damage modes to RA data, further investigations in less complex reinforced composite structures are needed.

Overall, the present findings serve as a basis for further analyses to enable integrity assessment and damage modes identification by AE for SFRC materials. It is envisioned that additional test configurations and an advanced artificial intelligence-based pattern recognition techniques relying on multi-variable classification (e.g., rise times, amplitudes, energy, peak frequency), instead of waveform analysis as adopted in this paper, may provide greater insight into damage feature identification using AE.

**Author Contributions:** Conceptualization, H.N., H.A., R.S., J.R. and P.M.; methodology, H.N. and H.A.; investigation, validation, formal analysis, H.N.; resources, J.R. and P.M.; data curation, writing—original draft preparation, H.N.; writing—review and editing, H.N. and P.M.; supervision, P.M.; project administration, funding acquisition, R.S., J.R. and P.M. All authors have read and agreed to the published version of the manuscript.

**Funding:** This research was funded by MITACS, grant number IT13015. The APC was funded through a Collaborative Research and Development Grant by the Natural Sciences and Engineering Research Council of Canada, with partner Shawcor Ltd., grant number CRDPJ 538383-18.

**Acknowledgments:** Authors would like to thank Luis Gonzales for his technical advice and providing the materials used for the experiments.

**Conflicts of Interest:** The authors declare no conflict of interest.

## References

1. Masuelli, M.A. Introduction of fibre-reinforced polymers—Polymers and composites: Concepts, properties and processes. In *Fiber Reinforced Polymers—The Technology Applied for Concrete Repair*; Masuelli, M.A., Ed.; IntechOpen: London, UK, 2013; pp. 3–40.
2. Mertiny, P. Leakage failure in fibre-reinforced polymer composite tubular vessels at elevated temperature. *Polym. Test* **2012**, *31*, 25–30. [[CrossRef](#)]
3. Simonen, F.A. Pressure vessels and piping systems: Reliability, risk and safety assessment. In *Ancillary Equipment and Electrical Equipment*; EOLSS Publications: Abu Dhabi, United Arab Emirates, 2010; Volume 1, Available online: <http://www.desware.net/sample-chapters/d09/e6-165-07-00.pdf> (accessed on 20 November 2021).
4. Scott, I.G.; Scala, C.M. A review of non-destructive testing of composite materials. *NDT Int.* **1982**, *15*, 75–86. [[CrossRef](#)]
5. Wevers, M.; Lambrihgs, K. Applications of acoustic emission for SHM: A review. In *Encyclopedia of Structural Health Monitoring*; Boller, C., Ed.; John Wiley & Sons, Ltd.: Chichester, UK, 2009; Available online: <https://onlinelibrary.wiley.com/doi/epdf/10.1002/9780470061626.shm011> (accessed on 20 November 2021).
6. Eitzen, D.G.; Wadley, H.N.G. Acoustic emission: Establishing the fundamentals. *J. Res. Nat. Bur. Stand.* **1984**, *89*, 75–100. [[CrossRef](#)] [[PubMed](#)]
7. Liu, Z.; Kleiner, Y. State-of-the-art review of technologies for pipe structural health monitoring. *IEEE Sens. J.* **2012**, *12*, 1987–1992. [[CrossRef](#)]
8. Mukhopadhyay, C.K.; Jayakumar, T.; Haneef, T.K.; Suresh Kumar, S.; Rao, B.P.C.; Goyal, S.; Gupta, S.K.; Bhasin, V.; Vishnuvardhan, S.; Raghava, G.; et al. Use of acoustic emission and ultrasonic techniques for monitoring crack initiation/growth during ratcheting studies on 304LN stainless steel straight pipe. *Int. J. Pres. Ves. Pip.* **2014**, *116*, 27–36. [[CrossRef](#)]

9. Ono, K.; Gallego, A. Research and applications of AE on advanced composites. In Proceedings of the 30th European Conference on Acoustic Emission Testing & 7th International Conference on Acoustic Emission, Granada, Spain, 12–15 September 2012; NDT.net: Bad Breisig, Germany.
10. Collins, D.J. Damage Detection in Composite Materials Using Acoustic Emission and Self-Sensing Fibres. Ph.D. Thesis, University of Birmingham, Birmingham, UK, 2010.
11. Ni, Q.Q.; Iwamoto, M. Wavelet transform of acoustic emission signals in failure of model composites. *Eng. Fract. Mech.* **2002**, *69*, 717–728. [[CrossRef](#)]
12. de Groot, P.J.; Wijnen, P.A.M.; Janssen, R.B.F. Real-time frequency determination of acoustic emission for different fracture mechanisms in carbon/epoxy composites. *Compos. Sci. Technol.* **1995**, *55*, 405–412. [[CrossRef](#)]
13. Ramirez-Jimenez, C.R.; Papadakis, N.; Reynolds, N.; Gan, T.H.; Purnell, P.; Pharaoh, M. Identification of failure modes in glass/polypropylene composites by means of the primary frequency content of the acoustic emission event. *Compos. Sci. Technol.* **2004**, *64*, 1819–1827. [[CrossRef](#)]
14. Amenabar, I.; Mendikute, A.; López-arraiza, A.; Lizaranzu, M.; Aurrekoetxea, J. Comparison and analysis of non-destructive testing techniques suitable for delamination inspection in wind turbine blades. *Compos. Part B-Eng.* **2011**, *42*, 1298–1305. [[CrossRef](#)]
15. Nikbakht, M.; Yousefi, J.; Hosseini-Toudeshky, H.; Minak, G. Delamination evaluation of composite laminates with different interface fiber orientations using acoustic emission features and micro visualization. *Compos. Part B-Eng.* **2017**, *113*, 185–196. [[CrossRef](#)]
16. Fotouhi, M.; Heidary, H.; Ahmadi, M. Characterization of composite materials damage under quasi-static three-point bending test using wavelet and fuzzy C-means clustering. *J. Compos. Mater.* **2012**, *46*, 1795–1808. [[CrossRef](#)]
17. Zhou, W.; Zhao, W.; Zhang, Y.; Ding, Z. Cluster analysis of acoustic emission signals and deformation measurement for delaminated glass fiber epoxy composites. *Compos. Struct.* **2018**, *195*, 349–358. [[CrossRef](#)]
18. Beheshtizadeh, N.; Mostafapour, A.; Davoodi, S. Three point bending test of glass/epoxy composite health monitoring by acoustic emission. *Alex Eng. J.* **2019**, *58*, 567–578. [[CrossRef](#)]
19. Liu, P.; Yang, J.; Peng, X. Delamination analysis of carbon fiber composites under hygrothermal environment using acoustic emission. *J. Compos. Mater.* **2017**, *51*, 1157–1571. [[CrossRef](#)]
20. Gutkin, R.; Green, C.J.; Vangrattanachai, S.; Pinho, S.T.; Robinson, P.; Curtis, P.T. On acoustic emission for failure investigation in CFRP: Pattern recognition and peak frequency analyses. *Mech. Syst. Signal. Pr.* **2011**, *25*, 1393–1407. [[CrossRef](#)]
21. Shateri, M.; Ghaib, M.; Svecova, D.; Thomson, D. On acoustic emission for damage detection and failure prediction in fiber reinforced polymer rods using pattern recognition analysis. *Smart Mater. Struct.* **2017**, *26*, 065023. [[CrossRef](#)]
22. Sikdar, S.; Mirgal, P.; Banerjee, S.; Ostachowicz, W. Damage-induced acoustic emission source monitoring in a honeycomb sandwich composite structure. *Compos. Part B-Eng.* **2019**, *158*, 179–188. [[CrossRef](#)]
23. Momon, S.; Godin, N.; Reynaud, P.; R’Mili, M.; Fantozzi, G. Unsupervised and supervised classification of AE data collected during fatigue test on CMC at high temperature. *Compos. Part A-Appl. S* **2012**, *43*, 254–260. [[CrossRef](#)]
24. Das, A.K.; Suthar, D.; Leung, C.K.Y. Machine learning based crack mode classification from unlabeled acoustic emission waveform features. *Cement. Concrete. Res.* **2019**, *121*, 42–57. [[CrossRef](#)]
25. Chandarana, N.; Martinez-Sanchez, D.; Soutis, C.; Gresil, M. Early damage detection in composites by distributed strain and acoustic event monitoring. *Procedia Eng.* **2017**, *188*, 88–95. [[CrossRef](#)]
26. Barile, C.; Casavola, C.; Pappaletta, G. Damage assessment of carbon fibre reinforced plastic using acoustic emission technique: Experimental and numerical approach. *Struct. Health Monit.* **2020**, *20*, 1090–1101. [[CrossRef](#)]
27. Oz, F.E.; Ersoy, N.; Lomov, S.V. Do high frequency acoustic emission events always represent fibre failure in CFRP laminates? *Compos. Part A Appl. Sci. Manuf.* **2017**, *103*, 230–235. [[CrossRef](#)]
28. Saeedifar, M.; Zarouchas, D. Damage characterization of laminated composites using acoustic emission: A review. *Compos. Part B* **2020**, *195*, 108039. [[CrossRef](#)]
29. Barile, C.; Casavola, C.; Pappaletta, G. Application of different acoustic emission descriptors in damage assessment of fiber reinforced plastics: A comprehensive review. *Eng. Fract. Mech.* **2020**, *235*, 107083. [[CrossRef](#)]
30. ASTM D7264; Standard Test Method for Flexural Properties of Polymer Matrix Composite Materials. ASTM International: West Conshohocken, PA, USA, 2007.
31. ASTM D2584; Standard Test Method for Ignition Loss of Cured Reinforced Resin. ASTM International: West Conshohocken, PA, USA, 2011.
32. Gillis, P.P. *Dislocation Motions and Acoustic Emissions*; Liptai, R., Harris, D., Tatro, C., Eds.; ASTM International: West Conshohocken, PA, USA, 1972.
33. Ali, H.Q.; Tabrizi, I.E.; Khan, R.M.A.; Tufani, A.; Yildiz, M. Microscopic analysis of failure in woven carbon fabric laminates coupled with digital image correlation and acoustic emission. *Compos. Struct.* **2019**, *230*, 111515. [[CrossRef](#)]
34. Alia, A.; Fantozzi, G.; Godin, N.; Osmani, H.; Reynaud, P. Mechanical behaviour of jute fibre-reinforced polyester composite: Characterization of damage mechanisms using acoustic emission and microstructural observations. *J. Compos. Mater.* **2019**, *53*, 3377–3394. [[CrossRef](#)]
35. Wolff-fabris, F.; Starzynski, K.; Altst, V. Identification of failure mechanisms of metallised glass fibre reinforced composites under tensile loading using acoustic emission analysis. *Compos. Part B Eng.* **2015**, *81*, 1–13.

36. Tabrizi, I.E.; Kefal, A.; Seyyed, J.; Zanjani, M.; Akalin, C.; Yildiz, M. Experimental and numerical investigation on fracture behavior of glass/carbon fiber hybrid composites using acoustic emission method and refined Zigzag theory. *Compos. Struct.* **2019**, *223*, 110971. [[CrossRef](#)]
37. Bohmann, T.; Schlamp, M.; Ehrlich, I. Acoustic emission of material damages in glass fibre-reinforced plastics. *Compos. Part B Eng.* **2018**, *155*, 444–451. [[CrossRef](#)]
38. Kalteremidou, K.; Murray, B.R.; Tsangouri, E.; Aggelis, D.G.; Hemelrijck, D.V.; Pyl, L. Multiaxial damage characterization of carbon/epoxy angle-ply laminates under static tension by combining in situ microscopy with acoustic emission. *Appl. Sci.* **2018**, *8*, 2021. [[CrossRef](#)]
39. Aggelis, D.G.; Barkoula, N.; Matikas, T.E.; Paipetis, A.S. Acoustic structural health monitoring of composite materials: Damage identification and evaluation in cross ply laminates using acoustic emission and ultrasonics. *Compos. Sci. Technol.* **2012**, *72*, 1127–1133. [[CrossRef](#)]